Atmos. Chem. Phys. Discuss., 6, 11597–11620, 2006
www.atmos-chem-phys-discuss.net/6/11597/2006/

Atmospheric Chemistry and Physics Discussions

Near-UV photolysis cross sections of CH_3OOH and $HOCH_2OOH$ determined via action spectroscopy

C. M. Roehl[1], Z. Marka[1,*], J. L. Fry[2,], and P. O. Wennberg[1,3]**

[1]Division of Geological and Planetary Sciences, California Institute of Technology, Pasadena, CA 91125, USA
[2]Arthur Amos Noyes Laboratory of Chemical Physics, California Institute of Technology, Pasadena, CA 91125, USA
[3]Division of Engineering and Applied Science, California Institute of Technology, Pasadena, CA 91125, USA
[*]now at: Columbia Astrophysics Laboratory, Columbia University, New York, NY 10027, USA
[**]now at: Department of Chemistry, University of California, Berkeley, Berkeley, CA 94720-1460, USA

Received: 18 October 2006 – Accepted: 2 November 2006 – Published: 20 November 2006

Correspondence to: C. M. Roehl (coleen@gps.caltech.edu)

Abstract

Knowledge of molecular photolysis cross sections is important for determining atmospheric lifetimes and fates of many species. A method and laser apparatus for measurement of these cross sections in the near-ultraviolet (UV) region is described. The technique is based on action spectroscopy, where the yield of a photodissociation product (in this case OH) is measured as a function of excitation energy. For compounds yielding OH, this method can be used to measure near-UV photodissociation cross section as low as 10^{-23} cm^2 molecule^{-1}. The method is applied to determine the photodissociation cross sections for methyl hydroperoxide (CH_3OOH; MHP) and hydroxymethyl hydroperoxide ($HOCH_2OOH$; HMHP) in the 305–365 nm wavelength range. The measured cross sections are in good agreement with previous measurements of absorption cross sections.

1 Introduction

Photolysis rates in the troposphere are determined by the magnitude of the absorption cross sections at wavelengths longer than 305 nm, the so-called "ozone cut-off". For many molecules, however, absorption cross sections have been measured only at shorter wavelengths where the cross sections are much larger and thus easier to quantify. In these studies, light passes through an absorption cell of known path length (l) and intensity is recorded at specific wavelengths (λ), both with the cell empty ($I_o(\lambda)$) and after sample has been added ($I(\lambda)$). Pressure measurements (N, in molecule cm^{-3}) are simultaneously taken and the absorption cross sections are determined by application of Beer-Lambert's law:

$$\sigma_{\mathrm{abs},\lambda} = \ln[I_o(\lambda)/I(\lambda)]/lN \quad (1)$$

Absorption measurements in the near-UV region are complicated by several problems. For many species, cross sections in this region are very small (on the order

of 10^{-23} cm^2 molecule^{-1} or less) but nevertheless contribute significantly to the atmospheric photodissocation rate. To measure these weak molecular absorbances, their contribution often must be separated from larger absorbance caused by impurities that are inevitably present in the sample analyzed. In many cases, the absorption of both the target molecule and the impurities are spectrally unstructured, making the separation difficult. In addition to these problems, determination of the atmospherically relevant quantity, the photodissociation cross section ($\sigma_{\mathrm{diss},\lambda}$), requires the separate measurement of the photodissociation quantum yield, ϕ_λ:

$$\sigma_{\mathrm{diss},\lambda} = \sigma_{\mathrm{abs},\lambda} \times \phi_\lambda \quad (2)$$

Photodissociation cross sections can be measured directly with a technique known as action spectroscopy. In this method, the molecule of interest is photolyzed and the yield of a photoproduct is monitored. For example, OH radical may be monitored via laser induced fluorescence (LIF). This detection scheme is especially advantageous since the OH product concentration is monitored against virtually zero background. By scanning the wavelength of the photolysis light source, the action spectrum (photodissociation cross section vs. wavelength) can be obtained. In cases where the photodissociation quantum yield is unity, $\sigma_{\mathrm{diss},\lambda}$=$\sigma_{\mathrm{abs},\lambda}$, action spectroscopy can be used to directly measure absorption cross sections.

An example that demonstrates the advantages of action spectroscopy over typical absorption measurements is the measurement of the cross section of HOBr above 400 nm. Standard absorption measurements are complicated by interferences from impurities introduced in the generation of HOBr (Orlando and Burkholder, 1995). Using action spectroscopy and OH LIF detection, however, Barnes et al. (1996) discovered a new absorption band around 440 nm arising from excitation to a triplet state that can dominate the atmospheric photodissociation of this molecule in the troposphere and lower stratosphere.

The aim of this study was to develop an accurate photodissociation cross section measurement methodology in the near-UV region based on action spectroscopy. In

this wavelength region, just above the ozone cut-off, the absorption spectra of many molecules of atmospheric importance have sizable "tails" which determine their photolysis lifetimes in the atmosphere.

We chose methyl- and hydroxymethyl- hydroperoxide as test molecules for this technique. Accurate near-UV absorption cross sections are required as photodissociation of these molecules is known to be important for determining OH concentrations. Such data is also useful in laboratory studies, where concentrations of these species are often measured by UV absorption. Yet, despite their importance, large uncertainties remain in the literature on these cross sections.

Methyl- and hydroxymethyl- hydroperoxide are the two most abundant atmospheric organic peroxides and act as sinks and temporary reservoirs for both HO_x and RO_x species. The transport of these species can have important regional and even global effects on radical concentrations (Jaegle et al., 1997). Peroxides are removed from the atmosphere by wet and dry deposition as well as by reaction with OH radicals or by photolysis:

$$\mathrm{ROOH} + \mathrm{OH} \rightarrow \text{ products} \quad (R1)$$

$$\mathrm{ROOH} + h\nu \rightarrow \text{ products} \quad (R2)$$

Hence atmospheric lifetimes, which are determined in part by these processes, will determine the role of these species in the transport of urban photochemistry to remote environments.

2 Experimental methodology

We observed the LIF signal from OH following the photolysis of the hydroperoxides in the 305–365 nm wavelength range. The measured OH LIF signal can be expressed as:

$$\mathrm{LIF}(\lambda) = c(\lambda)\phi(\lambda)\sigma(\lambda)[\mathrm{ROOH}], \quad (3)$$

where σ and ϕ describe the wavelength dependent absorption cross section and quantum yield, respectively, [ROOH] is the concentration of the given molecule, and $c(\lambda)$ is a wavelength dependent but species independent constant related to photon flux and pump-probe laser overlap volume.

The measured signals of MHP were converted to absolute cross sections using a reference species, hydrogen peroxide or H_2O_2, which has a well-known absorption cross section in this wavelength region (Nicovich and Wine, 1988). The photolysis quantum yield for H_2O_2 has been previously measured at 248 nm, where it dissociates to two OH radicals (ϕ=2) (Vaghjiani and Ravishankara, 1990). At longer wavelengths, such as in our studies, the OH quantum yield is also accepted to be 2 (Sander et al., 2003). Substituting the known cross sections for H_2O_2 (σ_{HOOH}) and ϕ_{HOOH}=2, the ratio of the laser-power-normalized LIF counts,

$$\frac{LIF_{peroxide}}{LIF_{HOOH}} = \frac{\phi_{peroxide}\sigma_{peroxide}[peroxide]}{\phi_{HOOH}\sigma_{HOOH}[HOOH]}, \quad (4)$$

is used to obtain the photolysis cross sections ($\phi\times\sigma$). By employing this ratio equation at every wavelength measured, the c(λ) constants cancel out of the equation making their difficult determination unnecessary. All peroxide concentrations were determined using FTIR spectroscopy.

The signals for MHP and H_2O_2 were measured back-to-back at each wavelength. For HMHP, however, the system required longer times to condition the walls, making switching between HMHP and H_2O_2 at each wavelength impractical. Instead, continuous HMHP spectra were obtained by scanning the photolysis laser from 312 to 357 nm. These spectra were normalized for laser power, small changes in the concentration of HMHP and H_2O_2 impurity (both as determined by FTIR), and changes in photon flux. Similar scans were performed for H_2O_2 before and after each HMHP scan. To account for any changes in the pump-probe laser overlap volume, our measured H_2O_2 cross sections were compared to the "accepted" H_2O_2 cross sections generated from the parameterization of Nicovich and Wine (1988). A wavelength dependent correction was

calculated and applied to our measured HMHP cross sectional values. Absolute HMHP cross sections were referenced to the σ_{HMHP} value of Bauerle and Moortgat (1999) at 320 nm (1.3×10^{-21} cm^2 molecule^{-1}).

Equation (3) holds true only if the OH LIF signal is taken just after the photolysis laser pulse. At longer times, the temporal profile of OH concentration decays, with a rate constant of $k=k_d+\Sigma k_i[i]$, where k_d is the rate coefficient for diffusion of OH out of the detection zone and k_i is the rate coefficient for the bimolecular reaction of OH with species i. If the total pressure in the sample cell is the same, k_d will not be different for the target and reference gas. Under the same experimental flow and pressure conditions, however, differences in the OH temporal profiles can arise from differing bimolecular rate constants of OH with the target and reference compounds. With fast electronics and high sensitivity (and thus limited concentrations of the peroxides), it is possible to limit the observational period to be sufficiently short that correction for the different OH loss in the flow tube is not required.

3 Instrumentation

Figure 1 depicts the laser system and the gas delivery scheme used in our experiments. A system of two lasers, with variable time delay, is used to produce the photolysis pump pulse (near-UV) and the OH LIF probe (282 nm). LIF signal is recorded using a photomultiplier tube operated in single photon counting mode. The gas mixtures are carried through a glass flow tube and detection block before transiting through a long pass FTIR cell for concentration determination.

3.1 Gas delivery, reaction chamber and FTIR cell

Gas-phase peroxides were generated by passing N_2 through a bubbler containing the organic peroxide or H_2O_2. Semiconductor grade H_2O_2 was obtained commercially (FMC Corporation) at 70% in H_2O, and used as purchased. MHP was synthesized

via a literature procedure (Vaghjiani and Ravishankara, 1989b). Synthesis of HMHP is based on the method described by Bauerle and Moortgat (1999). A low flow of N_2 is passed over 5 g paraformaldehyde powder (Aldrich) at 100°C and subsequently bubbled for ∼14 h through 7 mL 90–95% H_2O_2 (distilled from 70%) in H_2O maintained at 60°C. Excess H_2O_2 was maintained during the synthesis to avoid formation of *bis*-HMHP ($HOCH_2OOCH_2OH$). The resulting liquid sample is immediately placed in a glass bubbler for the experiments. To prevent injury in case of a peroxide explosion, the HMHP bubbler is housed in a Plexiglas box. Although efforts were made to consistently synthesize HMHP with the smallest amount of impurities, the presence of H_2O_2 impurity in our HMHP samples is seemingly unavoidable. Therefore, the sample is pumped on at highest possible pumping speed for several hours prior to photolysis experiments to remove remaining H_2O, HCOOH, and H_2O_2 contamination. The MHP and HMHP purities were checked by FTIR measurements.

A bulb of water behind a valve is connected to the top of the HMHP bubbler and outside of the sample box. After each experiment is finished, the peroxide residue is quenched with water prior to any handling. **Extreme caution should be exercised when working with concentrated samples of peroxides. The water quenching method is highly recommended; this was implemented after an explosion occurred when our seemingly empty sample vessel containing HMHP residue was vented to atmospheric pressure.**

The bubblers containing MHP and H_2O_2 were kept in ice water, while the HMHP bubbler was maintained at room temperature. In order to establish stable peroxide flows and constant pressures over the peroxides in the bubblers (∼400 Torr for MHP, ∼200 Torr for H_2O_2) over the timeframe of each measurement, mass flow controllers were used to set the N_2 flow over the bubbler (80 sccm for both MHP and H_2O_2 and 30 sccm for HMHP) and glass frits were used downstream of the bubblers. The MHP and H_2O_2 peroxide vapors then were mixed with an additional 200 sccm of N_2 upon entering a jacketed glass flow cell (50 cm long, 2.5 cm internal diameter, Teflon coated to minimize heterogeneous chemistry on the walls). Due to the rapid decomposition of

HMHP on the walls, was necessary to reduce the pressure of HMHP in the bubbler (to ∼30 Torr) and increase the flow rates in the inlet region. No N_2 gas was introduced. The peroxide flow entered the reaction chamber where it crossed the pump and probe laser beams. The output port of the reaction chamber lead to an 86 cm long double pass FTIR cell, an external cell connected to a Nicolet Magna-IR 560 FTIR interferometer. The flow tube, reaction chamber, and FTIR cell pressures were maintained around 30 Torr for MHP and H_2O_2; signal optimization occurred at ∼3 Torr for the HMHP system. H_2O_2 concentration was determined by fitting the obtained IR spectra with the H_2O_2 cross sections from the HITRAN database (Rothman et al., 2003).

The MHP concentration was determined from an absorption feature in the C-H stretch region at 2963.8 cm^{-1}, using a published absorption coefficient (ε) of 3.2×10^{-19} cm^2 $molecule^{-1}$ which was obtained at 0.0625 cm^{-1} theoretical resolution (Niki et al., 1983). The MHP concentrations used here were typically (1–10)$\times10^{14}$ molecule cm^{-3}. The HMHP concentration was determined from a peak in the C-O stretch region at 1049 cm^{-1}. A peak IR absorption coefficient (ε) of 3×10^{-19} cm^2 $molecule^{-1}$ was averaged from two literature values and employed here (Neeb, 1997; Bauerle and Moortgat, 1999). Typical concentrations of HMHP were (1–3)$\times10^{14}$ molecule cm^{-3} with H_2O_2 impurities of (2–20)$\times10^{12}$ molecule cm^{-3}. The concentration of the reference H_2O_2 was (2–12)$\times10^{14}$ molecule cm^{-3}.

3.2 Lasers and detection

The photolysis laser light was generated by sum frequency mixing the signal output of a Type-II BBO optical parametric oscillator (OPO) with the 1064 nm fundamental output of a pulsed Nd:YAG laser (Coherent Infinity 40–100). The 355 nm THG (third harmonic generation) output of the same Nd:YAG laser serves as the pump for the OPO (Wu et al., 1997). The frequency of the signal output of the OPO was continuously monitored by a pulsed wavemeter (Burleigh), from which the mixed near-UV wavelength is calculated. The OPO signal and Nd:YAG fundamental beams are brought together with a high frequency beam splitter and collinearly enter a Type-I BBO crystal used

for generating the near-UV beam. A Pellin-Broca prism spatially separates the various frequencies of light exiting this mixing crystal and also serves as a compensator for the directional beam changes as the mixing crystal is rotated. The mixing crystal and prism are mounted on calibrated and fully automated mechanical drives. For the mixed beam a power of >100 mW (at 100 Hz repetition rate) is easily achieved in the 305–365 nm wavelength range, with pulse length around 10 ns. During experiments, fluctuations in the laser power are continuously monitored by a photodiode, which is aligned in the path of the reflected portion of the UV beam from the CaF_2 Brewster angle input window of the detection cell. The photodiode signal is calibrated against a thermal power meter positioned at the optical exit (also a CaF_2 Brewster angle window).

The OH probe laser system consists of a frequency doubled Nd:YAG laser (Spectra Physics), which serves as the pump of a Rhodamine 6G dye laser (Lambda Physik). The Q-switch of the Nd:YAG laser is slaved with a variable delay to the photodissociation laser. The second harmonic UV output from this system (<1 μJ pulse energy, ~40 ns pulse width, tunable around 282 nm) excites the OH generated in the photolysis chamber. For the data reported here, the UV probe beam is tuned to the strongest OH LIF feature ($Q_{11}(1)+Q_{21}(1)+R_{22}(3)$ unresolved triplet of lines) in the $A^2\Sigma(v=1) \leftarrow X^2\Pi(v=0)$ band.

The pump and probe beams are spatially overlapped before crossing the flowing gas in the interaction volume. Photodissociation occurs via the lowest energy channel in MHP:

$$CH_3OOH + h\nu \rightarrow CH_3O + OH \qquad \lambda_{threshold}=645\,nm \qquad (R3)$$

Similarly, photolysis of HMHP is expected to proceed via:

$$HOCH_2OOH + h\nu \rightarrow HOCH_2O + OH. \qquad \lambda_{threshold}=1028\,nm \qquad (R4)$$

The OH relaxes via collisions with the N_2 bath gas to the v=0 state and fluorescence is observed at 309 nm ($A^2\Sigma(v=0) \rightarrow X^2\Pi(v=0)$) (Wennberg et al., 1994). The LIF signal is focused onto a bialkali photomultiplier tube mounted above the detection region, at

right angles to both the laser beams and the gas flow. A narrow-band interference filter centered at 310 nm is employed to reject scattered UV laser light.

A PC controls a National Instruments DA/AD board for digitizing the laser power measurements, and an SRS400 gated counter collects the LIF signal input from a photomultiplier tube, which is mounted above the interaction volume (crossing of gas flow and laser beams).

4 Results and discussion

Our experiments were aimed at directly determining the photolysis cross section of MHP and HMHP in the atmospherically important near-UV region. The quantum yield of OH in the atmospheric photolysis of both species is generally accepted to be unity e.g., Vaghjiani and Ravishankara (1990) at 248 nm for MHP. Thus, the near-UV photodissociation cross section from this experiment can be compared to previous absorption cross section measurements.

By varying the delay between the near-UV photolysis and the LIF probe laser pulses, we recorded the temporal profile of the OH photolysis product. Under our experimental flow conditions and concentrations, the OH lifetime in the detection region at 30 Torr is around 0.2 ms. Most of this decay is due to flow and diffusion of OH products from the detection zone. The other main source of OH signal decay is the bimolecular reaction of OH with the peroxides. Though the difference between the corresponding reaction rate constants is substantial (1.7×10^{-12} cm^3 $molecule^{-1}$ s^{-1} for ($OH+H_2O_2$) vs. 5.5×10^{-12} cm^3 $molecule^{-1}$ s^{-1} for ($OH+CH_3OOH$) Vaghjiani and Ravishankara, 1989b) for the concentrations used in our experiments this contributes minimal differences in the observed OH lifetime. (The rate constant for the $OH+HOCH_2OOH$ reaction has not been measured, but is assumed to be comparable.) The LIF data for the cross section measurements was taken 1 μs following the photodissociation pulse with a gate window of a 30 ns, thus differences in bimolecular decay constants do not yield any significant errors in the resulting relative photolysis cross sections.

The UV photolysis cross sections for MHP and HMHP as a function of wavelength are shown in Fig. 2, with tabulated results given in Tables 1 and 2. Our MHP work is compared to UV cross sections reported by Vaghjiani and Ravishankara (1989a) in the range between 300 and 365 nm and recent Matthews et al. (2005) between 355 and 405 nm while our HMHP data is compared with the values of Bauerle and Moortgat (1999) 300–360 nm.

The error bars in Fig. 2 represent the standard deviation from several measurements (3–10) at the same wavelength. Using ϕ=1, the measured absorption cross section values for MHP are 8–21% greater then the JPL recommendation. The data shown in Fig. 2a and Table 1 was obtained by taking reference measurements to hydrogen peroxide photolysis cross sections. Recent reevaluation of earlier hydrogen peroxide cross section measurement in the near-UV by Knight et al. (2002) resolved previous discrepancies in the H_2O_2 absorption cross section data around 340 nm. Thus the cross section values of Knight and coworkers in agreement with Molina and Molina (1981) as well as with the parameterization of Nicovich and Wine (1988), were used as reference for hydrogen peroxide near-UV absorption cross section, with a photolysis quantum yield of 2.

Our reported and Bauerle and Moortgat's literature HMHP data is given in Fig. 2b and Table 2. Reasonable agreement (within ∼20%) is observed between 310 and 340 nm, however, our HMHP cross section values remain lower than literature values, with a measured cross section at 350 nm which is 40% lower. This discrepancy might be due to the contribution of impurities in the data of Bauerle and Moortgat. However, it is also possible that there is an error in the H_2O_2 parameterization used, some unaccounted systematic change in error in c(λ), or some combination of these errors.

A significant source of uncertainty in our absolute photolysis cross section values results from uncertainties in the infrared extinction coefficients used. For MHP, the literature value was obtained with an FTIR instrument at a resolution of 0.0625 cm^{-1}. Our on-line FTIR used 0.25 cm^{-1} resolution. The differences in FTIR absorption of MHP at 2963.8 cm^{-1} at 0.0625 and 0.25 cm^{-1} (16% at ∼30 Torr) was determined from

spectra obtained at high resolution using a Bruker (IFS 125HR) spectrometer and a correction factor was applied. A similar correction was not necessary in the case of HMHP as no resolution effect was observed between the resolutions of 0.5 cm^{-1} (used to obtain the referenced literature value) and 1.0 cm^{-1} (used in this study).

Figure 3 shows the experimentally obtained ratio of photolysis cross section of hydrogen peroxide and methyl hydroperoxide up to 365 nm. An independent measurement of absorption cross section above 350 nm is not available for H_2O_2. As the wavelength increases above 350 nm, the H_2O_2/MHP cross section ratio decreases below 2, indicating that MHP more efficiently dissociates at higher wavelengths than hydrogen peroxide. Some additional data was taken at decreased temperatures (260 K) in the high wavelength tail. Above 350 nm H_2O_2/MHP cross section ratio increased significantly at lower temperatures hinting at possible reduced MHP photodissociation at colder temperatures that needs to be studied further.

Taking advantage of the wide wavelength range of our laser system we also searched for peroxide absorption features in the 430–550 nm wavelength region, by removing the frequency mixing stage and using the signal output of the OPO. As expected, no LIF signal was detected for either MHP or HMHP. This finding is consistent with unpublished electronic excited state calculations of HMHP (J. Lane, private communication).

In order to evaluate the atmospheric importance of UV photolysis, the ground-level total UV photolysis rates across the 300–400 nm window (between the ozone cutoff and where the cross sections become small and hence atmospherically negligible) were determined for MHP and HMHP data collected here as well as literature data. By using the log-linear dependence of the absorption cross section versus wavelength observed for many molecules (Sander et al., 2003), cross sections were extrapolated out to 400 nm. Cross sections were then multiplied by solar actinic fluxes calculated at the Earth's surface (0 km and 40° zenith angle) for each wavelength (Finlayson-Pitts and Pitts, 1986) to get the partial photolysis rates J_λ:

$$J_\lambda = \sigma(\lambda)I(\lambda)d\lambda[s^{-1}\,nm^{-1}] \quad (5)$$

These partial photolysis rates J_λ as a function of wavelength are compared in Fig. 4.

Note that the photolysis rates for both species are dominated by absorption occurring near 330 nm. A coarse box integration of the band is then calculated by summing all these partial photolysis rates, to derive the total photolysis rate J:

$$J = \sum_{\lambda} J_{\lambda}[s^{-1}] \quad (6)$$

The integrated UV photolysis in the region 300–400 nm is likely to account for most of the UV photolysis of these peroxides.

The calculated total photolysis rates for MHP are $1.29\times10^{-6}\,s^{-1}$ and $1.10\times10^{-6}\,s^{-1}$, using the cross sections (plus extrapolations) determined by this work and that of Vaghjiani and Ravishankara (1989a), respectively, suggesting an 18% increase in the total UV photolytic loss over previous estimates. This increase is reduced to 10% if the long wavelength (λ>360 nm) cross sections of Matthews et al. (2005) are substituted into the summations instead of the extrapolated values. Matthews et al. use a similar OH LIF technique and compare back-to-back OH yields at desired photolysis wavelengths with that from a 355 nm reference beam. Using the 355 nm cross section value measured by Vaghjiani and Ravishankara and normalizing for laser power gives them an estimate of the absorptions cross sections at the longer wavelengths. Similar calculations for HMHP resulted in photolysis rates of $9.08\times10^{-7}\,s^{-1}$ and $1.08\times10^{-6}\,s^{-1}$, using the cross sections determined by this work and that of Bauerle and Moortgat (1999), respectively. This suggests a decrease in the total UV photolytic loss for HMHP from 300–400 nm of 16%.

5 Conclusions

The photolysis cross sections of methyl- and hydroxymethyl-hydroperoxide were determined via action spectroscopy in the 305–365 nm region. By directly measuring photolysis cross sections we determined the product of quantum yield and absorption cross section – the information of most importance in atmospheric photochemistry.

Using these photolysis cross sections, we calculated the total photolytic loss of MHP ($1.3\times10^{-6}\,s^{-1}$) and HMHP ($9.1\times10^{-7}\,s^{-1}$) in the UV region between 300 and 400 nm. Advances in laser technology make possible a tunable laser source in the 300–365 nm region, just above the ozone cutoff, where both solar flux and absorption coefficients of atmospherically relevant molecules are large, giving rise to considerable photodissociation rates in the troposphere. As our results show, the methodology described in this paper easily enables the measurement of photodissociation cross sections in the high $10^{-23}\,cm^2\,molecule^{-1}$ for OH producing species. At most wavelengths, we used significantly lower photolysis laser powers than our instrument is capable of producing (in order to extend the lifetime of our crystal surfaces) hence, the current measurement limit of our instrument for near-UV photolysis cross sections is estimated in the low $10^{-23}\,cm^2\,molecule^{-1}$ region.

Acknowledgements. The authors thank the National Science Foundation (ATM-0432377) and the Massachusetts Institute of Technology, Air Quality Models Project (R824970-01-0) for support of this research.

References

Barnes, R. J., Lock, M., Coleman, J., and Sinha, A.: Observation of a new absorption band of HOBr and its atmospheric implications, J. Phys. Chem., 100, 453–457, 1996.

Bauerle, S. and Moortgat, G. K.: Absorption cross-sections of $HOCH_2OOH$ vapor between 205 and 360 nm at 298 K, Chem. Phys. Lett., 309, 43–48, 1999.

Finlayson-Pitts, B. J. and Pitts Jr., J. N.: Atmospheric Chemistry: Fundamentals and Experimental Techniques, Wiley, New York, 1986.

Jaegle, L., Webster, C. R., May, R. D., Scott, D. C., Stimpfle, R. M., Kohn, D. W., Wennberg, P. O., Hanisco, T. F., Cohen, R. C., Proffitt, M. H., Kelly, K. K., Elkins, J., Baumgardner, D., Dye, J. E., Wilson, J. C., Pueschel, R. F., Chan, K. R., Salawitch, R. J., Tuck, A. F., Hovde, S. J., and Yung, Y. L.: Evolution and stoichiometry of heterogeneous processing in the Antarctic stratosphere, J. Geophys. Res.-Atmos., 102, 13 235–13 253, 1997.

Knight, G., Ravishankara, A. R., and Burkholder, J. B.: UV absorption cross sections of HO_2NO_2 between 343 and 273 K, Phys. Chem. Chem. Phys., 4, 1432–1437, 2002.

Matthews, J., Sinha, A., and Francisco, J. S.: The importance of weak absorption features in promoting tropospheric radical production, Proceedings of the National Academy of Sciences of the USA, 102, 7449–7452, 2005.

Molina, L. T. and Molina, M. J.: UV absorption cross-sections of HO_2NO_2 vapor, J. Photochem., 15, 97–108, 1981.

Neeb, P., Sauer, F., Horie, O., and Moortgat, G. K.: Formation of hydroxymethyl hydroperoxide and formic acid in alkene ozonolysis in the presence of water vapour, Atmos. Environ., 31, 1417–1423, 1997.

Nicovich, J. M. and Wine, P. H.: Temperature-dependent absorption cross-sections for hydrogen-peroxide vapor, J. Geophys. Res., 93, 2417–2421, 1988.

Niki, H., Maker, P. D., Savage, C. M., and Breitenbach, L. P.: A Fourier-transform infrared study of the kinetics and mechanism for the reaction HO + CH_3OOH, J. Phys. Chem., 87, 2190–2193, 1983.

Orlando, J. J. and Burkholder, J. B.: Gas-phase UV visible absorption-spectra of HOBr and Br_2O, J. Phys. Chem., 99, 1143–1150, 1995.

Rothman, L. S., Barbe, A., Benner, D. C., Brown, L. R., Camy-Peyret, C., Carleer, M. R., Chance, K., Clerbaux, C., Dana, V., Devi, V. M., Fayt, A., Flaud, J. M., Gamache, R. R., Goldman, A., Jacquemart, D., Jucks, K. W., Lafferty, W. J., Mandin, J. Y., Massie, S. T., Nemtchinov, V., Newnham, D. A., Perrin, A., Rinsland, C. P., Schroeder, J., Smith, K. M., Smith, M. A. H., Tang, K., Toth, R. A., Vander Auwera, J., Varanasi, P., and Yoshino, K.: The HITRAN molecular spectroscopic database: edition of 2000 including updates through 2001, J. Quant. Spect. Rad. Trans., 82, 5–44, 2003.

Sander, S. P., Friedl, R. R., Golden, D. M., Kurylo, M. J., Huie, R. E., Orkin, V. L., Moortgat, G. K., Ravishankara, A. R., Kolb, C. E., Molina, M. J., and Finlayson-Pitts, B. J.: Chemical Kinetics and Photochemical Data for Use in Atmospheric Studies, Eval. 14, National Aeronautics and Space Administration, Jet Propulsion Laboratory, and California Institute of Technology, Pasadena, CA, 2003.

Vaghjiani, G. L. and Ravishankara, A. R.: Absorption cross-sections of CH_3OOH, H_2O_2, and D_2O_2 vapors between 210 nm and 365 nm at 297 K, J. Geophys. Res., 94, 3487–3492, 1989a.

Vaghjiani, G. L. and Ravishankara, A. R.: Kinetics and mechanism of OH reaction with

CH_3OOH, J. Phys. Chem., 93, 1948–1959, 1989b.

Vaghjiani, G. L. and Ravishankara, A. R.: Photodissociation of H_2O_2 and CH_3OOH at 248 nm and 298 K: Quantum yields for OH, O(^3P) and H(^2S), J. Chem. Phys., 92, 996–1003, 1990.

Wennberg, P. O., Cohen, R. C., Hazen, N. L., Lapson, L. B., Allen, N. T., Hanisco, T. F., Oliver, J. F., Lanham, N. W., Demusz, J. N., and Anderson, J. G.: Aircraft-borne, laser-induced fluorescence instrument for the in-situ detection of hydroxyl and hydroperoxyl radicals, Rev. Sci. Instrum., 65, 1858–1876, 1994.

Wu, S., Blake, G. A., Sun, Z. Y., and Ling, J. W.: Simple, high-performance type II beta-BaB2O4 optical parametric oscillator, Appl. Opt., 36, 5898–5901, 1997.

Table 1. Absorption cross sections as a function of wavelength for methyl hydroperoxide. Extrapolated cross sections are indicated by an asterisk (*). †Note: Matthews et al.'s data is normalized to the 355 nm cross section value measured by Vaghjiani and Ravishankara.

Wavelength (nm)	Cross section (cm^2 $molecule^{-1}$) MHP this work	Vaghijiani and Ravishankara (1989a)	Matthews et al. (2005)
300		4.13 E–21	
305	3.72 E–21	3.13 E–21	
310		2.39 E–21	
315	1.98 E–21	1.82 E–21	
320	1.53 E–21	1.37 E–21	
325	1.19 E–21	1.05 E–21	
330	9.00 E–22	7.90 E–22	
335	7.10 E–22	6.10 E–22	
340	5.50 E–22	4.70 E–22	
345	4.30 E–22	3.50 E–22	
350	3.30 E–22	2.70 E–22	
355	2.49 E–22*	2.10 E–22	2.10 E–22†
360		1.60 E–22	
365		1.20 E–22	1.14 E–22
370			7.50 E–23
375			5.20 E–23
380			4.00 E–23
385			
390			1.40 E–23
395			7.00 E–24
400			6.00 E–24

Table 2. Absorption cross sections as a function of wavelength for hydroxymethyl hydroperoxide.

Wavelength (nm)	Cross section (cm^2 $molecule^{-1}$) HMHP this work	Bauerle and Moortgat (1999)
300		4.00 E–21
305		2.90 E–21
310	2.24 E–21	2.20 E–21
315	1.65 E–21	1.80 E–21
320	1.22 E–21	1.30 E–21
325	9.03 E–22	1.00 E–21
330	6.67 E–22	7.30 E–22
335	4.92 E–22	5.90 E–22
340	3.64 E–22	4.50 E–22
345	2.69 E–22	3.60 E–22
350	1.98 E–22	2.80 E–22
355	1.47 E–22	2.20 E–22
360	1.08 E–22	1.70 E–22

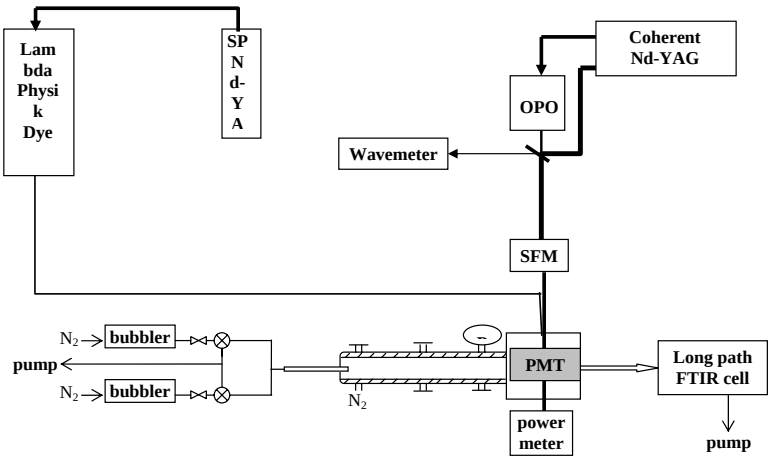

Fig. 1. Experimental setup for photolysis cross section measurements in the near-UV region.

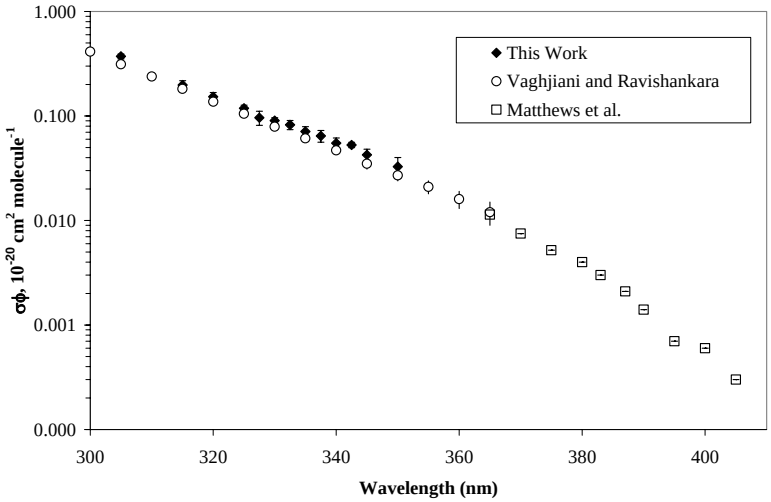

Fig. 2a. Measured photolysis cross sections of methyl hydroperoxide (solid diamonds) compared with current JPL evaluation values for absorption cross sections of Vaghjiani and Ravishankara (1989a) (open circles) and with recent longer wavelength measurements by Matthews et al. (2005) (open squares).

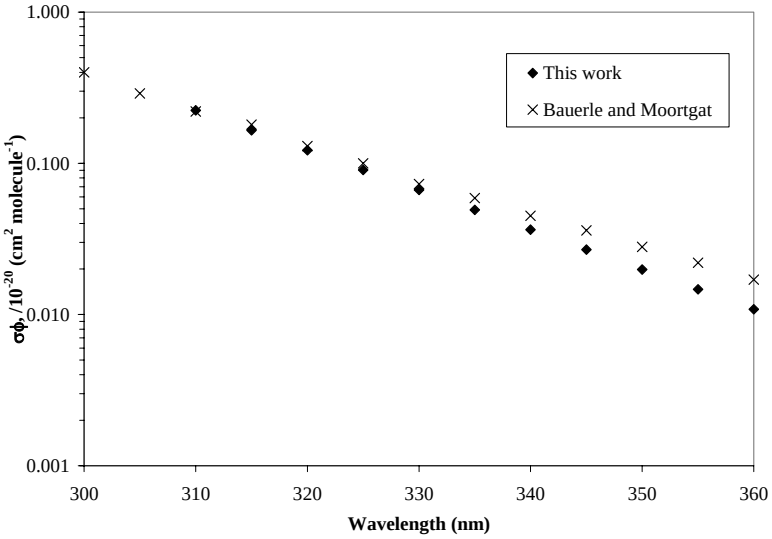

Fig. 2b. Measured photolysis cross sections of hydroxymethyl hydroperoxide (solid diamonds) compared with values from Bauerle and Moorgat (1999) (crosses).

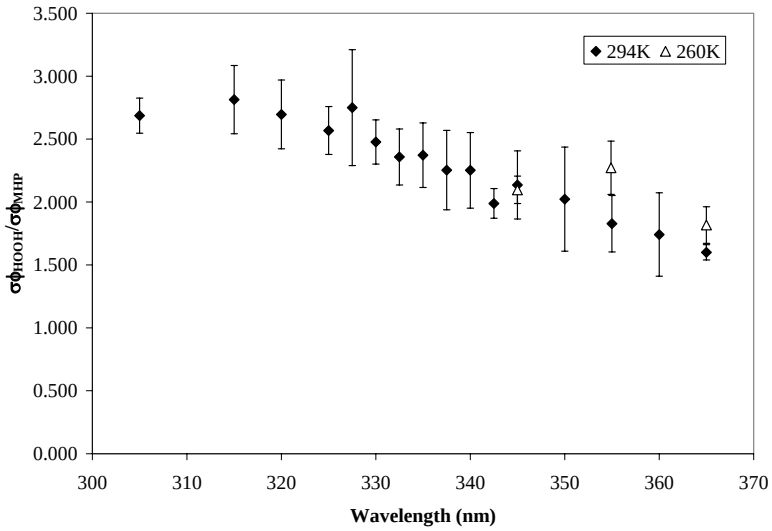

Fig. 3. Ratio of hydrogen peroxide and methyl hydroperoxide photolysis cross sections versus wavelength (solid diamonds taken at 294 K; open triangles at 260 K).

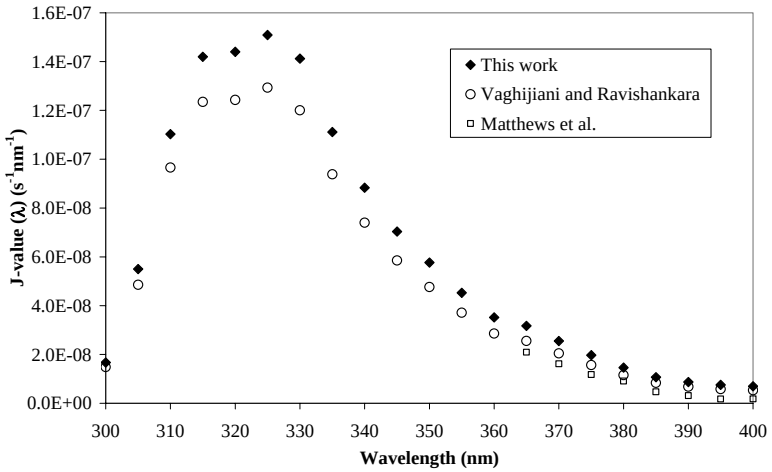

Fig. 4a. Partial photolysis rates for methyl hydroperoxide: using measured cross sections plus extrapolated values between 355–400 nm (solid diamonds), using cross sections of Vaghjiani and Ravishankara (1989a) plus extrapolation between 370–400 nm (open circles), and using long wavelength measurements by Matthews et al. (2005) (open squares).

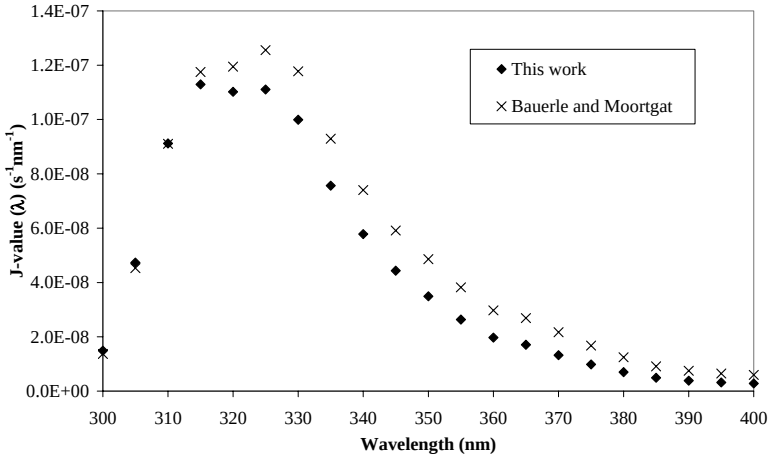

Fig. 4b. Partial photolysis rates for hydroxymethyl hydroperoxide: using measured cross sections plus extrapolated values between 365–400 nm (solid diamonds) and using cross sections of Bauerle and Moortgat (1999) plus extrapolation between 365–400 nm (crosses).